Whittier College
Poet Commons

Physics | Faculty Publications & Research

2006

The Parsec-Scale Jet of PKS 0637-752

Philip G. Edwards

B. Glenn Piner
Whittier College, gpiner@whittier.edu

Steven J. Tingay

James E. Lovell

Jun Kataoka

See next page for additional authors

Follow this and additional works at: https://poetcommons.whittier.edu/phys

Recommended Citation

Edwards, P. G., Piner, B., Tingay, S. J., Lovell, J. E., Kataoka, J., Ojha, R., & Murata, Y. (2006). The Parsec-Scale Jet of PKS 0637-752. *Publications of the Astronomical Society of Japan, 58*, 233. Retrieved from https://poetcommons.whittier.edu/phys/38

This Article is brought to you for free and open access by the Faculty Publications & Research at Poet Commons. It has been accepted for inclusion in Physics by an authorized administrator of Poet Commons. For more information, please contact library@whittier.edu.

Authors

Philip G. Edwards, B. Glenn Piner, Steven J. Tingay, James E. Lovell, Jun Kataoka, Roopesh Ojha, and Yasuhiro Murata

This article is available at Poet Commons: https://poetcommons.whittier.edu/phys/38

PASJ: Publ. Astron. Soc. Japan **58**, 233–241, 2006 April 25
© 2006. Astronomical Society of Japan.

The Parsec-Scale Jet of PKS 0637−752

Philip G. EDWARDS,[1,2] B. Glenn PINER,[3] Steven J. TINGAY,[4] James E. J. LOVELL,[5]
Jun KATAOKA,[6] Roopesh OJHA,[5] and Yasuhiro MURATA[1,2]
[1]*The Institute of Space and Astronautical Science, Japan Aerospace Exploration Agency,*
3-1-1 Yoshinodai, Sagamihara, Kanagawa 229-8510
edwards.philip@jaxa.jp
[2]*Department of Space and Astronautical Science, The Graduate University for Advanced Studies,*
3-1-1 Yoshinodai, Sagamihara, Kanagawa 229-8510
[3]*Department of Physics and Astronomy, Whittier College, 13406 E. Philadelphia St., Whittier, CA 90608, USA*
[4]*Centre for Astrophysics and Supercomputing, Swinburne University of Technology, PO Box 218, Hawthorn, VIC 3122, Australia*
[5]*Australia Telescope National Facility, CSIRO, PO Box 76, Epping, NSW 1710, Australia*
[6]*Department of Physics, Tokyo Institute of Technology, 2-12-1 Ookayama, Meguro-ku, Tokyo 152-8551*

(Received 2005 July 27; accepted 2005 November 13)

Abstract

Chandra observations of the quasar PKS 0637−752 during its checkout phase resulted in the unexpected detection of a luminous kiloparsec-scale X-ray jet. The apparent superluminal speed of this jet on the parsec-scale, based on two VSOP and four ground-based observations, has proven crucial to understanding the X-ray production in the arcsec-scale jet. We present here for the first time the full details of the ground-based observations used to determine the parsec-scale jet speed, describe the results of a third VSOP observation, and examine the reported jet speed in the light of more recent ground-based VLBI observations. We find some evidence of increased source activity coincident with extrapolated epochs of jet component ejection, although the monitoring of the source is relatively sparse and the ejection epochs are not tightly constrained. We also construct the spectral energy distribution for the nucleus of PKS 0637−752 and show that it can be modelled well in terms of a one-zone synchrotron self-Compton model of an electron-positron jet with a Doppler factor of ~ 10, consistent with the results of the VLBI observations.

Key words: galaxies: quasars: individual (PKS 0637−752) — radio continuum: galaxies — techniques: interferometric

1. Introduction

One of the surprises of the Chandra X-ray Observatory mission has been the observation of luminous X-ray jets in an appreciable number of active galactic nuclei (Sambruna et al. 2004; Marshall et al. 2005). This was, in a sense, Chandra's first discovery, as the "point source" selected for the first checkout phase observations, PKS 0637−752, was revealed to have a bright X-ray jet extending $10''$ from the nucleus (Schwartz et al. 2000; Chartas et al. 2000), coincident with a previously known radio jet (Tingay et al. 1998).

PKS 0637−752 is a bright radio quasar, with a total flux density at 4.8 GHz of ~ 7 Jy. The kiloparsec-scale structure is shown in figure 1: a jet extends $\sim 10''$ to the west before bending sharply to the north-west, whereas to the east, a single hot-spot is seen $\sim 10''$ from the core (Tingay et al. 1998; Schwartz et al. 2000; Chartas et al. 2000). The first VLBI image showed the parsec-scale jet extending over 4 milliarcsec (mas) and closely aligned with the kpc-scale jet to the west (Tingay et al. 1998).

A first epoch VSOP observation was made at 5 GHz on 1997 November 21 as part of a sample of gamma-ray-quiet active galactic nuclei (AGN) for comparison with a sample of southern EGRET detected AGN (Tingay et al. 2000). A second epoch observation was made in 1999 August to coincide with Chandra checkout phase observations (Lovell et al. 2000; Tingay et al. 2002). The data from these two VSOP observations were combined with data from ground-only VLBI observations, with the resulting component motions (Lovell et al. 2000) placing tight constraints on the jet angle to the line of sight, and in turn on models for the X-ray emission from the kpc-scale jet (Schwartz et al. 2000; Chartas et al. 2000; Tavecchio et al. 2000; Celotti et al. 2001; Georganopoulos et al. 2005).

Schwartz et al. (2000) considered several possible origins for the X-ray emission in the kpc-scale jet, favouring a synchrotron self-Compton model, but noting that this entailed significant departures from commonly assumed equipartition and/or homogeneity conditions. Tavecchio et al. (2000) and Celotti, Ghisellini, and Chiaberge (2001) showed, however, that inverse Compton scattering of cosmic microwave background radiation provided a good fit to the data, if the Doppler factor inferred for the pc-scale jet still applied to the kpc-scale jet. Georganopoulos et al. (2005) have noted that the kpc-scale knot in PKS 0637−752 provides an ideal opportunity to resolve the long-standing question of the matter content of jets.

In this paper, we give in section 2 the first detailed account of the ground-based observations used to derive the pc-scale jet speeds, together with details of other observations, and in section 3 we re-examine the component speeds. Possible evidence for activity accompanying the extrapolated epochs of component ejection is presented in section 4, and in section 5

Downloaded from https://academic.oup.com/pasj/article/58/2/233/1514666 by guest on 04 November 2020

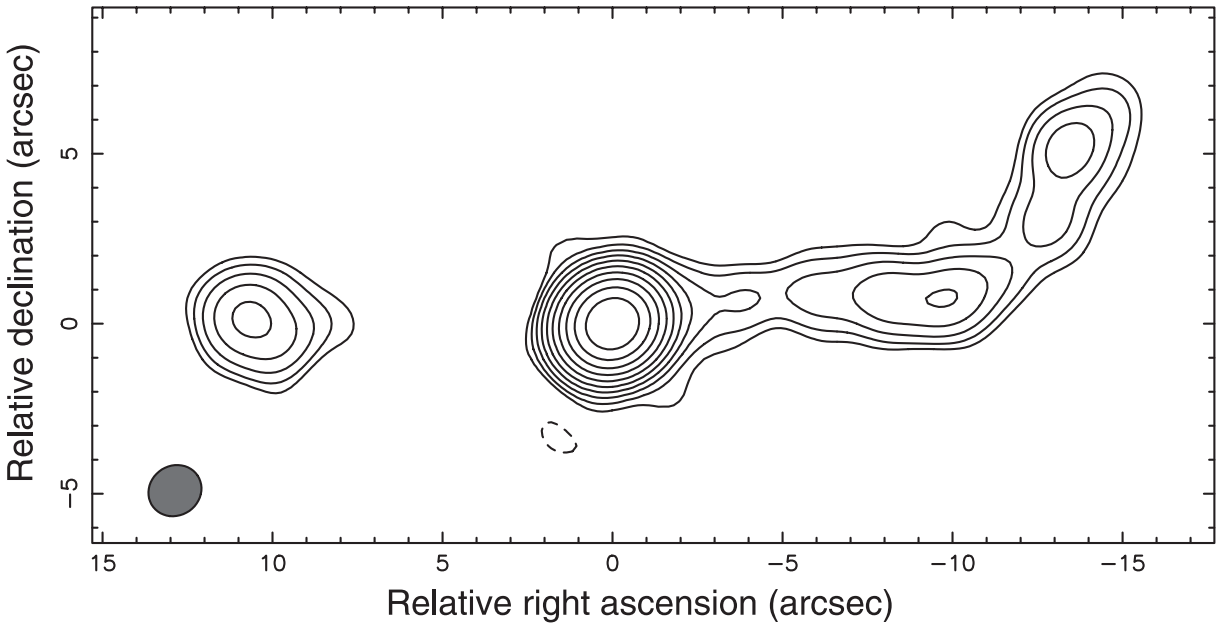

Fig. 1. ATCA image at 4.816 GHz of the kiloparsec-scale structure of PKS 0637−752 made by combining the data from the internal ATCA baselines of the VSOP observations in 1999 August and September (see table 1). The image peak is 6.12 Jy beam^{-1}, and the beam, shown at bottom left, is $1\farcs6 \times 1\farcs46$ (FWHM) at a position angle of $-56°$. Contour levels are −1 (dashed), 1, 2, 4, ..., 512 × 6 mJy beam^{-1}, with this base level corresponding to three times the residual noise level in the image. Chartas et al. (2000) note that at 4.8 GHz the arcsec core accounts for 90.2% of the total flux density, the inner western jet (before the bend at 10″ from the core), 4.5%, the outer western jet, 2.4%, and the eastern hotspot, 2.9%.

we derive the spectral energy distribution (SED) of the core and present a model for the SED constrained by the parameters determined in the preceding sections.

At a redshift of 0.654 (Bechtold et al. 2002), 1 mas corresponds to 6.94 pc for a cosmological model with H_0 = 71 km s^{-1} Mpc^{-1}, $\Omega_M = 0.27$, and $\Omega_{vac} = 0.73$. At this distance, a motion of 1 mas yr^{-1} corresponds to an apparent speed 37.4c.

2. Observations and Modelfits

Details of all the observations considered in this paper are presented in table 1. As the 1997 VSOP observation has been described by Tingay et al. (2000) and the 1999 August observation by Tingay et al. (2002), we omit details of these observations here. In the next subsection we describe the four geodetic observations which were used together with these two VSOP observations to derive the component speeds in PKS 0637−752 by Lovell et al. (2000). In following subsections we briefly describe an earlier SHEVE observation from 1993 (Tingay et al. 1998), a third VSOP observation in 1999 September, and a more recent Australian Long Baseline Array (LBA) observation from 2002 July (Ojha et al. 2004).

Table 1. Details of the VLBI observations considered in this paper.

Date	Observation type	Frequency (GHz)	Bandwidth (MHz)	Telescopes*	Reference
1993 May 15	SHEVE	4.851	1.8	AT, Ho, Mp, Pa, Pr	Tingay et al. 1998
1995 Feb 13	Geodetic	8.381	16	Fo, Hh, Ho, Oh, Sa, Ti	
1995 Jul 12	Geodetic	8.381	16	Fo, Hh, Ho, Sa, Ti	
1995 Oct 12	Geodetic	8.381	16	Fo, Hh, Ho, Oh, Sa, Ti	
1996 Jul 25	Geodetic	8.596	16	Fo, Hh, Ho, Sa	
1997 Nov 21	VSOP	4.962	32	AT, Hh, Mp, HALCA	Tingay et al. 2000
1999 Aug 19	VSOP	4.800	32	AT, Hh, Ho, Mp, HALCA	Tingay et al. 2002
1999 Sep 12	VSOP	4.930	32	AT, Hh, HALCA	
2002 Jul 19	Geodetic	8.426	8	AT, Cd, Hh, Ho, Mp, Pa	Ojha et al. 2004

* Telescopes are: AT — Australia Telescope Compact Array; Cd — Ceduna, Australia, 30 m; Fo — Fortaleza, Brazil, 14 m; Hh — Hartebeesthoek, South Africa, 26 m; Ho — Hobart, Tasmania, 26 m; Mp — Mopra, Australia, 22 m; Pa — Parkes, Australia, 64 m; Pr — Perth (ESA), Australia, 27 m; Oh — O'Higgins, Antarctica, 9 m; Sa — Santiago, Chile, 12 m; Ti — Tidbinbilla (DSS-45), Australia, 34 m.

Downloaded from https://academic.oup.com/pasj/article/58/2/233/1514666 by guest on 04 November 2020

2.1. Geodetic Observations

Data from the four 8 GHz observations made in 1995 and 1996 were extracted from the geodetic VLBI archive of the United States Naval Observatory. These observations were fringe-fitted and calibrated in AIPS as described in Piner and Kingham (1998), and imaged in Difmap using natural weighting. Modelfits to these data were made in Difmap. Circular Gaussian components were used except for the 1995 October and 1999 August data sets, where elliptical Gaussians were found to provide a significantly better fit. In modelfitting the VSOP observations, HALCA data were upweighted by a factor of 50 so that the space baselines were treated appropriately in the Difmap modelfitting process (see, e.g., Piner et al. 2000).

Images from the four geodetic and two VSOP observations used by Lovell et al. (2000) to derive the jet component speeds are presented in figure 2, with the locations of modelfit components marked. Details of the image parameters are given in table 2, where a, b, and ϕ have their usual meanings of FWHM beam major axis and minor axis, and position angle respectively. The weighting refers to the two parameters used in the Difmap task `uvweight`. The first of these parameters is the bin-size in (u, v)-grid pixels within which neighboring visibilities are summed, with a bin-size greater than zero corresponding to uniform weighting. The second parameter is the exponent used for additional weighting (beyond the reciprocal of the summed visibilities) by amplitude errors. Results of the modelfits to the images are given in table 3.

2.2. The 1993 May SHEVE Observation

PKS 0637−752 was observed with the Southern Hemisphere VLBI Experiment (SHEVE) in 1993 May, with the resulting image presented by Tingay et al. (1998). Although no modelfit to the image was presented, inspection of the image (figure 4 in Tingay et al. 1998) reveals that a model containing the core and three jet components provides a good representation. The core distances determined in this way are plotted in figure 3.

2.3. The 1999 September VSOP Observation

In addition to the two VSOP observations described previously, a third VSOP observation was made at 4.9 GHz over 12 hr on 1999 September 12. The observation was conducted in the standard VSOP observing mode (Hirabayashi et al. 2000). Unfortunately, out of the ground telescopes originally scheduled only the ATCA and Hartebeesthoek were able to participate. As a result, the shortest baselines in this observation were 150 Mλ (with baselines to HALCA extending to 470 Mλ). In addition, two tracking passes scheduled for the first half of the observation were not successful, with HALCA data being obtained during two $\sim$ 1 hr tracking passes with the Robledo tracking station in the second half of the observation.

Phase self-calibration was limited to the two HALCA tracking passes, and amplitude self-calibration was not possible. Given the paucity of the data, we elected to image the data in Difmap and determine component positions based on the clustering of CLEAN components. This approach resulted in the detection of C4, C5, and C6 in addition to the core. The core distances of the three components were all within 0.1 mas of those determined for the VSOP observation of 1999 August 19. (The interval of 24 days between these epochs corresponds to an expected shift due to component motions of $\sim$ 0.02 mas.) Position angles were also generally consistent, with the largest difference, 12°, being for C6, the component closest to the core, as might be expected. As an additional check, we imported the modelfit for the 1999 August data into Difmap and compared the phases and amplitudes of visibility points against that for the 1999 September observation using `projplt`, finding good agreement. Nevertheless, given the superior quality of the August observation, we adopt the modelfits from that observation for calculating the component motions, with the September observation serving to confirm our confidence in the fidelity of that model.

2.4. The 2002 July LBA Observation

PKS 0637−752 was one of 69 southern sources observed at 8.4 GHz by Ojha et al. (2004). The observation was made as a series of snapshots with the Australian Long Baseline Array and Hartebeesthoek. The resulting image, shown in figure 1 of Ojha et al. (2004), clearly shows the core and a component with a north–south elongation $\sim$ 4.5 mas from the core. The modelfit in table 4 of Ojha et al. (2004) contains an elliptical Gaussian component at the core and two circular Gaussians 4.5 and 5.2 mas to the west. The latter component is not apparent in the image with, it is now realized, its position being influenced by an unmodelled residual to the north–west of the component visible in the image. A revised modelfit uses a single Gaussian to model the jet component, a circular Gaussian of 0.40 Jy with a FWHM of 0.51 mas located 4.5 mas from the core at a PA of −93° (Ojha, private communication).

3. Component Motions

The jet component identifications are listed together with details of the modelfit components in table 3. We emphasize that the modelfitting has been undertaken with the prime aim of locating the component core positions. In several cases the modelfits have converged to physically improbable representations — a point source for C2 in 1995 February, and linear features for the core and C3 in 1999 August — but we are satisfied that the locations of these features are sufficiently accurate for our purposes. Also, we note that the comparison of snapshot observations with longer astronomical observations, and observations at two frequencies, must be undertaken with caution. The apparent absence of C3 in the 1996 July image, for example, is not unexpected given the much higher rms noise level in this image (see table 2).

The modelfit positions are plotted in figure 3, together with those for the components in the SHEVE and LBA observations. The uncertainties in component locations were determined by projecting the beam major axis onto the line joining the component to the core. One quarter of the projected beam was adopted as the uncertainty for all observations. The comparison of component locations between the 1999 August and September VSOP observations described in subsection 2.3 indicates that this is a somewhat conservative assumption for these longer observations.

Downloaded from https://academic.oup.com/pasj/article/58/2/233/1514666 by guest on 04 November 2020

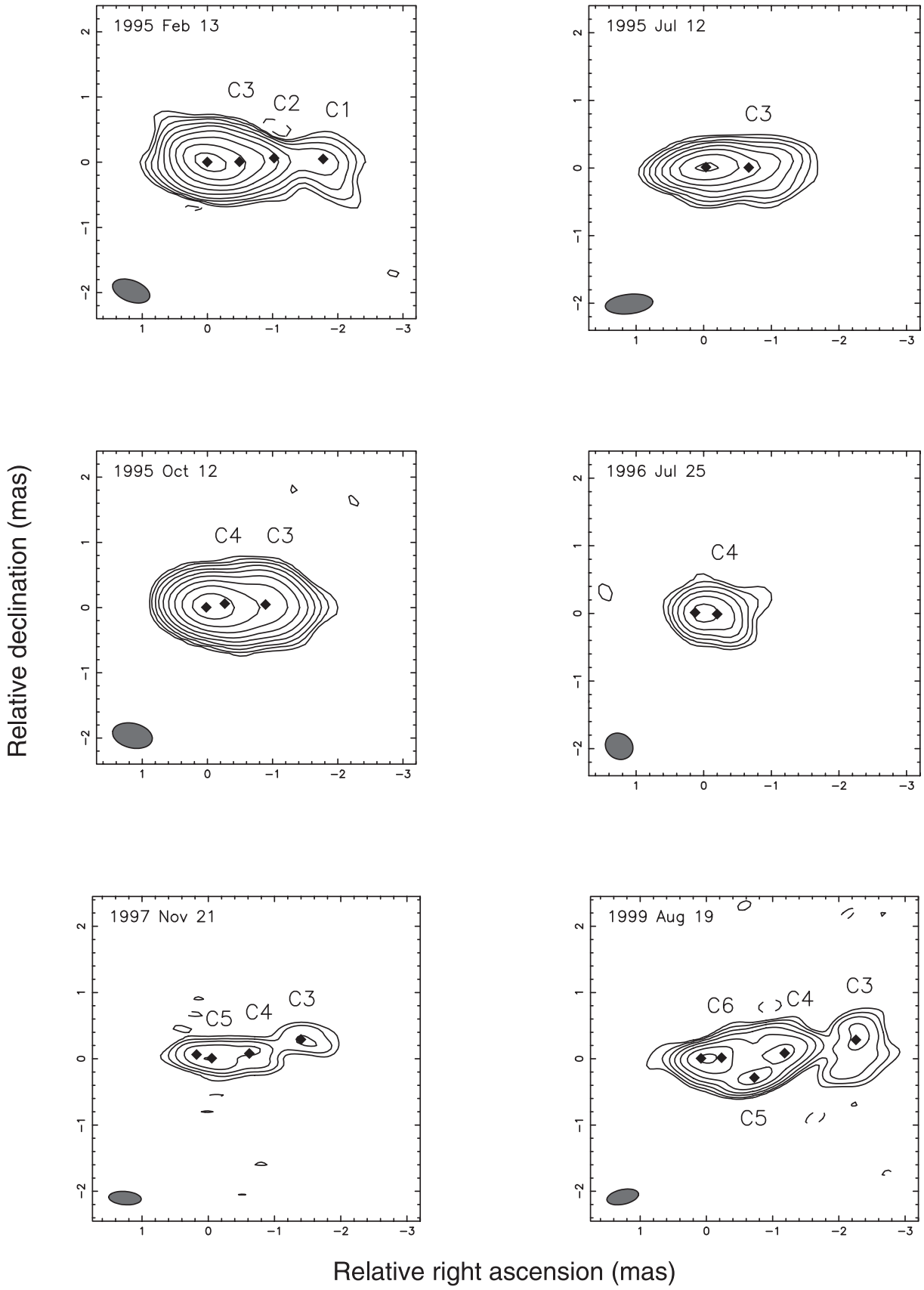

Fig. 2. Images from the first four geodetic and two VSOP observations. In each image the lowest contour on each image is 3 times the rms value, which is given in table 2, with successive contours a factor of 2 higher. The positions of modelfit components are marked, and the details of each component are given in table 3.

Downloaded from https://academic.oup.com/pasj/article/58/2/233/1514666 by guest on 04 November 2020

Table 2. Parameters of the images in figure 2.

Date	Beam size and orientation			Weighting	Peak flux	rms noise
	a (mas)	b (mas)	ϕ (deg)		(Jy)	(mJy)
1995 Feb 13	0.60	0.33	70	0, −2	1.93	1.8
1995 Jul 12	0.71	0.29	−84	0, −2	2.83	6.5
1995 Oct 12	0.62	0.38	77	0, −2	1.77	1.4
1996 Jul 25	0.42	0.37	56	0, −2	2.91	22.0
1997 Nov 21	0.49	0.20	86	2, 0	0.54	11.0
1999 Aug 19	0.49	0.22	−78	2, 0	0.62	2.8

Table 3. Modelfit results for the images in figure2.

Date	Flux density (Jy)	r (mas)	θ (deg)	a (mas)	a/b	ϕ (deg)	Identification
1995 Feb 13	2.33	0.00	0	0.27	1.00		Core
	1.26	0.49	−89	0.42	1.00		C3
	0.17	1.03	−87	0.00	1.00		C2
	0.08	1.78	−89	0.27	1.00		C1
1995 Jul 12	3.37	0.00	0	0.19	1.00		Core
	1.05	0.63	−91	0.36	1.00		C3
1995 Oct 12	1.66	0.00	0	0.19	1.00		Core
	0.86	0.29	−79	0.47	0.29	30	C4
	0.97	0.91	−87	0.59	0.82	89	C3
1996 Jul 25	1.85	0.00	0	0.04	1.00		Core
	2.67	0.33	−94	0.22	1.00		C4
1997 Nov 21	0.21	0.00	0	0.07	1.00		Core
	0.94	0.24	−104	0.33	1.00		C5
	0.63	0.80	−89	0.30	1.00		C4
	0.29	1.59	−82	0.31	1.00		C3
1999 Aug 19	0.58	0.00	0	0.22	0.00	43	Core
	1.05	0.31	−88	0.71	0.48	−45	C6
	0.49	0.86	−110	0.35	0.44	−77	C5
	0.88	1.26	−86	0.65	0.44	−71	C4
	0.28	2.36	−83	0.86	0.00	7	C3

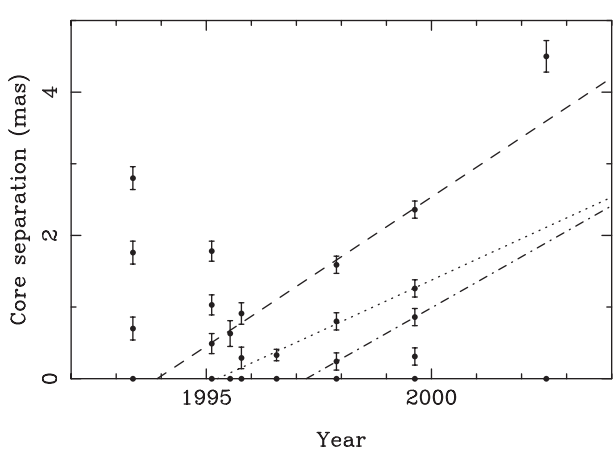

Fig. 3. Core distances of jet components at each epoch. The component motions derived by Lovell et al. (2000) are shown for C3 (dashed line), C4 (dotted), and C5 (dash-dot).

The component speeds inferred by Lovell et al. (2000) from the first four geodetic and two VSOP observations are also plotted: (0.41 ± 0.03), (0.29 ± 0.05), and $(0.35 \pm 0.09)\,\mathrm{mas\,yr^{-1}}$ for C3, C4, and C5, respectively. The weighted average of these corresponds to $(13.3 \pm 1.0)\,c$ for the cosmological model assumed here. This in turn yields a lower limit to the bulk Lorentz factor of $\Gamma_{\min} = 13.3$, and an upper limit to the line of sight of $\theta_{\max} = 8.^\circ 6$. [For the $H_0 = 50$, $q_0 = 0$ model adopted by Schwartz et al. (2000), the corresponding values are $\Gamma_{\min} = 17.8$ and $\theta_{\max} = 6.^\circ 4$.]

Comparison of the 1993 May observation with the 1995 February geodetic observation suggests that the component 0.7 mas from the core in the SHEVE observation can be identified with C2 in the latter, with an implied speed similar to that inferred to C4. This would further suggest that the component 1.7 mas from the core is associated with C1, with only marginal evidence for any motion between the two epochs. We note, however, that the larger uncertainties in the core distances of the 1993 observation, from both the lower angular resolution and the manner in which the core distances were

Downloaded from https://academic.oup.com/pasj/article/58/2/233/1514666 by guest on 04 November 2020

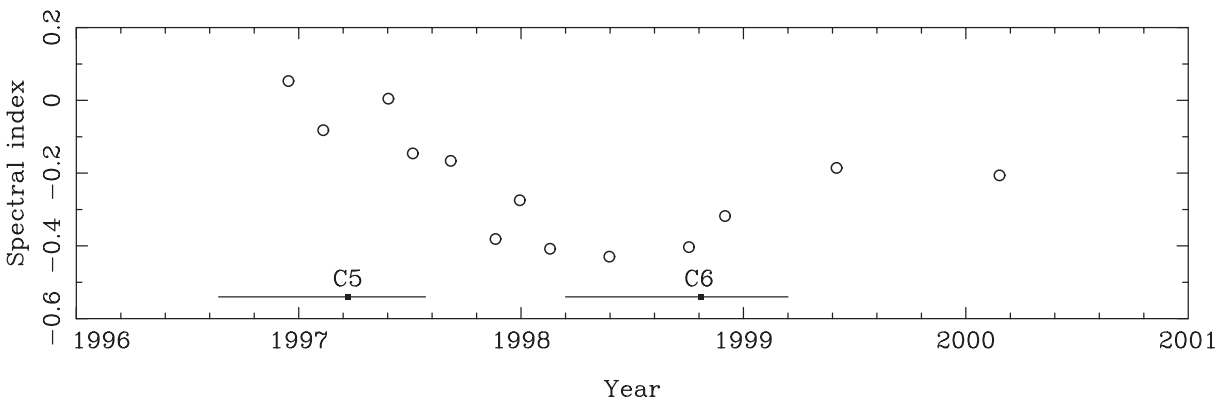

Fig. 4. The 4.8 to 8.4 GHz spectral index determined from 6 km baseline correlated flux densities as part of the ATCA monitoring program of Tingay et al. (2003). Errors in the spectral indices are comparable to the symbol size. The times of the ejection epochs of C5 and C6 are indicated at the bottom of the figure. For C5 the time range corresponds to the $1\,\sigma$ uncertainties in the ejection epoch. For C6 the time range was conservatively estimated using the speed of C4 with the upper limit of the component core distance, and the speed of C3 with the lower limit of the core distance.

derived, coupled with the fact that C1 is the weakest of all components listed in table 3, preclude any firm conclusions about the motion of this component.

As mentioned above, the third VSOP observation is too close to the 1999 August observation to provide any further constraints on the component motions. The 2002 July observation is however very interesting in this regard. The apparent non-detection of C4 and C5 at this epoch may well be related to the snapshot nature of the observation. The limited data and sparse (u, v) coverage result in a strong "striping" in full-resolution images, and so a conservative approach has been adopted in the imaging and modelfitting of the data. The single jet component identified in the 2002 July observation lies significantly above the extrapolated motion of C3. The north–south extension of this component is similar to that seen for C3 in the 1999 August epoch, lending confidence to the identification of this component with C3. Alternative models, such as a rapid fading of C3 and pronounced brightening of C2 or C1, weaker components not detected since 1995, appear far less likely. The formal component position is consistent with a departure from linear ballistic motion. However, given the preceding comments, we do not feel that this single observation constitutes sufficiently strong grounds to consider this possibility further. We simply conclude that the previously determined speed for C3 represents a firm lower limit to a linear motion for this component.

As such, rather than using the weighted mean of three components, the properties of the parsec-scale jet can be reliably based on the speed of C3 alone: a speed of $(0.41 \pm 0.03)c$, or $(15.3 \pm 1.1)c$, and hence $\Gamma > 15.3$, and $\theta < 7\overset{\circ}{.}5$. [For the cosmology adopted by Schwartz et al. (2000) the speed is $20.5\,c$, and $\theta_{\rm max} = 5\overset{\circ}{.}6$.]

4. Component Ejection Epochs

Extrapolating the component motions back in time allows the ejection epoch to be inferred. These are 1993.91 (with a $1\,\sigma$ range of 1993.61 to 1994.17) for C3, 1995.25 (1994.81 to 1995.57) for C4, and 1997.22 (1996.64 to 1997.57) for C5. C6 was only detected at two closely spaced epochs and so no speed has been measured for it. However, both the weighted speed for the other components and the speed for C3 alone suggest an ejection epoch in the latter part of 1998 or early 1999.

It is generally believed that the ejection of a new superluminal component is accompanied by behavior observable in single dish observations, such as flux density increases, with a general flattening of spectral indices, and changes in the polarization characteristics (e.g., Jorstad et al. 2001). Although there has been no long-term monitoring of PKS 0637−752 covering the entire time range of the VLBI observations, there are a number of programs which have spanned some of the periods of interest.

PKS 0637−752 was monitored at four frequencies at 15 epochs with the ATCA between 1996 February and 2000 February (Tingay et al. 2003). The monitoring was conducted as several snapshots, over a several-day period — too few to image the source reliably, but sufficient to determine the flux density on the 6 km baselines of the ATCA. Comparison of the images presented in Chartas et al. (2000) with the ATCA monitoring reveal that not all the flux is being recovered, but indicate that the 6 km flux densities are a good measure of the arcsec-scale core flux density. In figure 4 we plot the spectral index between 4.8 and 8.4 GHz. The spectral index generally steepens for the first two years, then rises again, peaking in mid-1999. Furthermore, we note that the highest fractional polarization at 8.6 GHz, 1.9%, was measured in 1999 February. This behavior is consistent with the ejection of C5 in late 1996 or early 1997 and C6 in late 1998 or early 1999.

PKS 0637−752 was part of the high precision relative photometric optical observations undertaken with the 0.6 m telescope at Observatório do Pico dos Dias, Brazil, by Garcia et al. (1999). The CCD based monitoring enabled observations accurate at the 0.02 mag level. PKS 0637−752 was observed at 9 epochs between 1993 November and 1997 May, covering the ejection period of C4. There is a notable departure from the general trend between observations at 1995.8 and 1996.3, when the source increased by 0.14 mag. (This is a modest increase compared to flares of a magnitude or more seen on occasions in other AGN, but is a significant increase for this source over

Downloaded from https://academic.oup.com/pasj/article/58/2/233/1514666 by guest on 04 November 2020

the monitoring period.) Although outside the 1σ error range of the extrapolated ejection epoch of C4 (1994.81 to 1995.57), if physically associated it would suggest a later ejection epoch for C4 (as this optical increase occurred after the extrapolated ejection epoch) and, subsequently, a component speed closer to that for C3.

Tornikoski et al. (1996) describe a SEST monitoring program of 155 extragalactic radio sources at 3 mm and 1.3 mm. PKS 0637−752 was monitored at 18 epochs at 3 mm and 8 epochs at 1.3 mm between 1988 April and 1994 June. A prominent outburst was detected in SEST monitoring of the source at 3 mm in 1988, with measured flux densities of (2.64 ± 0.31) Jy on October 16 and (7.90 ± 0.35) Jy on December 3. Immediately preceding (1988 August 23) and subsequent (1989 February 1) epochs reproduce the general levels of these two epochs, confirming that they are not affected by one-off systematic errors. The first 1.3 mm measurement, (2.58 ± 0.41) Jy, was made in 1988 December and was the largest 1.3 mm flux density observed for this source. There are no VLBI observations from this period. However, if this outburst was to mark the ejection epoch of the 1.8 mas component seen in the 1993 observation, a speed of $\sim 0.39\,\mathrm{mas\,yr^{-1}}$, or $14.5\,c$, is implied, consistent with that of C3. Kellermann et al. (2004) note, as we observe for the components in PKS 0637−752, that the speeds shown by separate jet components in a source are generally consistent.

These conclusions for enhanced activity associated with component ejections are necessarily somewhat speculative, as the monitoring of PKS 0637−752 is incomplete and relatively sparse. Nevertheless, the monitoring does indicate that PKS 0637−752 has displayed occasions of significant variability in the past, and that these can plausibly be related to the ejection epochs of new VLBI jet components.

5. Jet Alignment and Collimation

As noted by Schwartz et al. (2000), the 8.6 GHz ATCA image shows the kpc-scale jet emerging from the core at a PA of $-82°$ and maintaining this PA until $\sim 7''$ from the core, where it gradually bends toward the south, reaching a PA of $-86°$ (as measured from the core) at a distance of $10''$. As measured from the initial kpc-scale jet direction, this is a bend, in projection, of $\sim 10°$.

As indicated in table 3, the parsec-scale jet components display a range of PAs, generally around $-87°$. Component C5 is a notable exception, being detected at three epochs (including 1999 September) at PAs $< -100°$. As illustrated by the multi-epoch monitoring of 110 AGN by Kellermann et al. (2004), the components in most jets move in the general direction of an established jet, with non-radial motion, or clear bends, seen in the trajectories of fewer components. Observations of PKS 0637−752 to date have neither the temporal spacing nor sensitivity to determine whether the trajectories of components like C5 ultimately bend to become collimated with the kpc-scale jet, as seen, for example, in 3C 279 (Homan et al. 2003), or whether such components are intrinsically shorter lived.

The component speeds for C3, of at least $(0.41 \pm 0.03)\,\mathrm{mas\,yr^{-1}}$, and C4, $(0.29 \pm 0.05)\,\mathrm{mas\,yr^{-1}}$, are formally inconsistent, and this may well reflect intrinsic effects in the ejection of discrete components at different times. We note in passing, however, that if all components have the same bulk Lorentz factor of $\Gamma = 15.8$ (i.e., $\beta = 0.998\,c$) then the observed apparent speeds are observed for angles to the line of sight of $4\overset{\circ}{.}7$ for C3 and $9\overset{\circ}{.}1$ for C4. While a change of angle of $4\overset{\circ}{.}4$ is not inconsistent with the observed range of PAs observed for the parsec-scale components, the comparison is not straightforward due to projection effects.

It is clear from the summed component flux densities in table 3 that we are only recovering between $\sim 35\%$ and $\sim 65\%$ of the "core" flux density as measured on the arcsec scale (with calibration uncertainties likely to make a significant contribution to this apparently wide range). It is natural to suspect the remainder lies in jet structure intermediate between the mas and arcsec scales, i.e., intermediate between the scales able to be probed with the LBA and ATCA respectively. An instrument with a wide range of scaled baselines, like the planned Square Kilometer Array (Schilizzi 2004), would enable a study of the jet collimation and bending on these scales.

6. Spectral Energy Distribution

6.1. SED of the Kiloparsec-Scale Jet

Considerable effort has gone into understanding the physical processes responsible for the production of X-rays in the kpc-scale jet. The SED of the knot WK7.8 (see Chartas et al. 2000; Tavecchio et al. 2000) reveals that the X-ray emission cannot have a synchrotron origin as the optical flux is an order of magnitude below an interpolation between the radio and X-ray data. Tavecchio et al. (2000) and Celotti, Ghisellini, and Chiaberge (2001) have demonstrated that Compton scattering of the cosmic microwave background can explain X-ray emission if Doppler factors of around 10 are present, suggesting that the jets stay relativistic from the pc-scale to kpc-scale.

This is consistent with the apparent speeds of the parsec-scale jet components: in the following subsection we examine whether such a Doppler factor is consistent with a model for the SED of the nucleus.

6.2. SED of the Core

We assume an electron-positron jet and adopt the simple one-zone synchrotron self-Compton (SSC) model (see, e.g., Kataoka et al. 2002) to determine under what conditions the observed SED of the core can be reproduced. In this model, the radiation is due to a homogeneous jet component moving with a bulk Lorentz factor Γ, at an angle to the line of sight of θ, where these are constrained by the VLBI observations.

The model assumes that the low-energy synchrotron component and the high-energy SSC components arise from the same electron population with a Lorentz factor γ_p. The SSC spectrum is self-consistently calculated based on the parameters above, assuming an electron population of the form $N(\gamma) \propto \gamma^s \exp(-\gamma/\gamma_\mathrm{p})$, where s is conventionally assumed to be ~ -2.

We adopt $R = 10^{17}$ cm, based on the timescale of the 3 mm outburst seen by Tornikoski et al. (1996), and a Doppler factor of 10, consistent with the VLBI speeds. The millimeter data

Downloaded from https://academic.oup.com/pasj/article/58/2/233/1514666 by guest on 04 November 2020

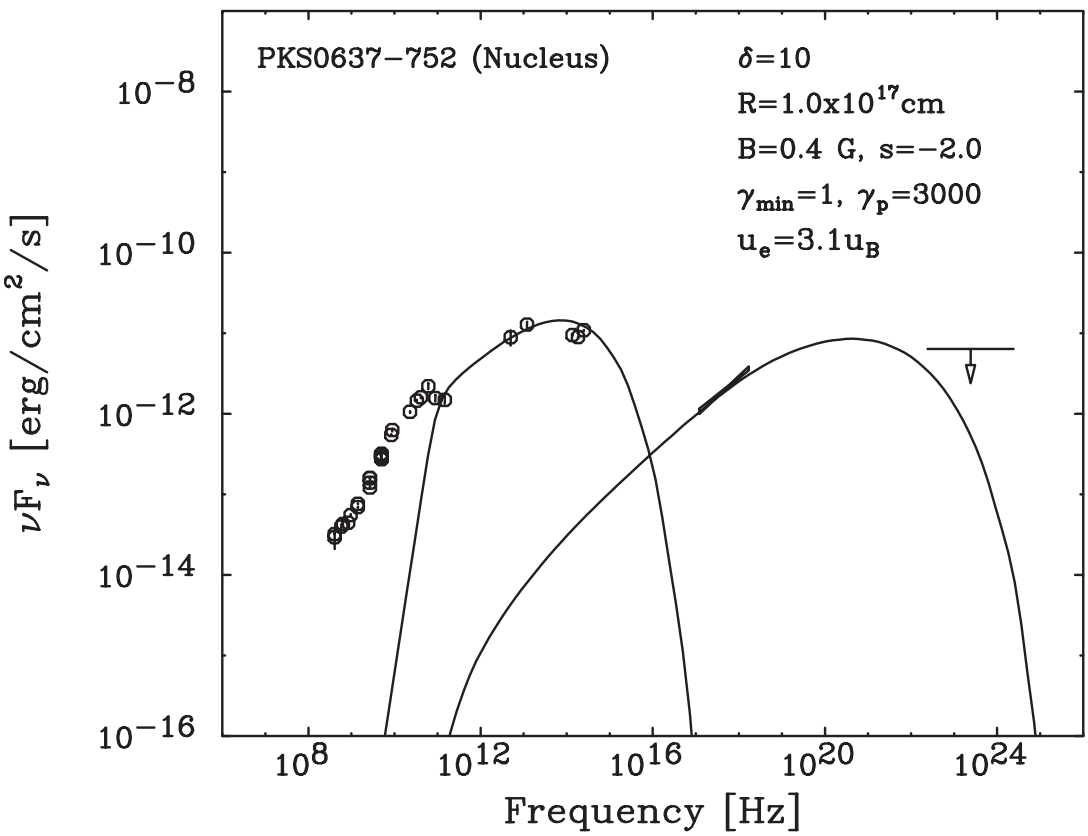

Fig. 5. Spectral energy distribution for the core of PKS 0637−752. See text for details.

in figure 5 are from WMAP (Bennett et al. 2003) and SEST (Beasley et al. 1997). The X-ray data are based on an analysis of data in the ASCA archive (see also, Yaqoob et al. 1998) but the spectrum and flux are consistent with the more recent Chandra observations (Chartas et al. 2000). The EGRET 2σ upper limit for $E > 100\,\mathrm{MeV}$ of $0.4 \times 10^{-7}\,\mathrm{cm^{-2}\,s^{-1}}$, is from phase I combined data (Fichtel et al. 1994) and we assume an E^{-2} spectrum. Other data points are from NED.[1]

The solid line in figure 5 shows the fit, yielding derived parameters $B = 0.4\,\mathrm{G}$ and $\gamma_\mathrm{p} = 3000$. Assuming $\gamma_\mathrm{min} = 1$ yields a ratio of electron/positron energy density, u_e, to magnetic field energy density, u_B, of 3.1. If we increase R by a factor of three, the resulting best fit yields $B = 0.1\,\mathrm{G}$, $s = -1.8$ and $\gamma_\mathrm{p} = 3500$, with $u_\mathrm{e}/u_\mathrm{B} = 11$. Alternatively, for a Doppler factor of 20, which is comparable to the $\delta = 17.4$ derived by Georganopoulos et al. (2005) to minimize the jet power in an electron-positron jet, $B = 0.02\,\mathrm{G}$, $s = -1.8$, $R = 5 \times 10^{17}$ and $\gamma_\mathrm{p} = 4000$, with $u_\mathrm{e}/u_\mathrm{B} = 100$.

The one-zone SSC model provides a good fit to the data above 10^{11} Hz. The fit below this frequency is poor, however this is a recognised characteristic of one-zone modelfits for AGN (see, e.g., Kataoka et al. 2002). The radio emission is assumed to be produced in a significantly larger volume than the SSC component of the SED. A value for R of 10^{17} cm corresponds to an angular size of 0.005 mas, well below the angular resolution of our observations. Although the VLBI images indicate the presence of a number of pc-scale components, each of which could be contributing to the SSC component of the SED, the addition of extra components to the model allows too many degrees of freedom, and so we follow the standard assumption that the source can be modelled by, or that the high energy emission is dominated by, a single component.

Furthermore, although the model assumes the X-ray emission is dominated by inverse Compton emission from the jet component, we cannot rule out a contribution from the accretion disk. For a $10^8\,M_\odot$ black hole, the Eddington luminosity for the nucleus would be similar to the observed value, $\sim 10^{46}\,\mathrm{erg\,s^{-1}}$, in which case the accretion disk component could be significant. However, as the X-ray spectrum is featureless (Chartas et al. 2000), and as the jet emission is boosted by a factor of δ^4, where the Doppler factor is most likely ~ 10, the assumption that the jet component is dominant can be readily justified.

Celotti, Ghisellini, and Chiaberge (2001) also present a model for the core emission. They assume $R = 5 \times 10^{16}$ cm, $B = 4\,\mathrm{G}$, $\Gamma = 20$, and $\theta = 5^\circ$ (thus $\delta = 9.9$). Their model incorporates inverse Compton scattering from external radiation fields as well as SSC and as a result has two peaks in the inverse Compton domain, though this region is currently poorly constrained observationally. Though both models fit the observational data equally well, we feel ours has the merit of a lower magnetic field (in part due to the larger value of R). Celotti, Ghisellini, and Chiaberge (2001) invoke a cold proton component for the jet to boost its kinetic power. Georganopoulos et al.

[1] ⟨http://nedwww.ipac.caltech.edu/⟩.

Downloaded from https://academic.oup.com/pasj/article/58/2/233/1514666 by guest on 04 November 2020

(2005) proposed observational tests to determine the matter content of jets, and we note that the results of Spitzer observations recently reported by Uchiyama et al. (2005) do in fact argue against pure electron-positron jets. Further observational tests will be able to be made in the hard X-ray region up to hundreds of keV with the Hard X-ray Detector of Suzaku, and above 20 MeV with GLAST, as the two SEDs differ in these regions.

7. Summary

We have compiled data from six ground-based observations and three VSOP observations to study the evolution of the parsec-scale jet. The third VSOP observation provides independent confirmation of the model derived from the 1999 August VSOP observation, and the 2002 July ground-based observation suggests that the well-constrained speed of C3 can be reliably used to define the properties of the parsec-scale jet; an apparent speed of $(15.3 \pm 1.1)c$ (for the cosmology we have assumed), $\Gamma_{\rm min} = 15.3$, and $\theta_{\rm max} = 7\overset{\circ}{.}5$. At face value, the 2002 July observation suggests either a higher speed or an acceleration of the component motion, but additional observations are required before these possibilities can be considered in more detail.

We have compared the extrapolated component ejection epochs with data from monitoring programs which included PKS 0637−752, and find there is some evidence of the increased core flux densities and polarized flux densities expected to accompany the birth of a new parsec-scale component.

Finally, we have constructed the spectral energy distribution for the core and find it can be well modeled by a one-zone synchrotron self-Compton model assuming a homogeneous, electron-positron dominated jet component with properties consistent with the VLBI results, and with an acceptable value for the derived magnetic field strength and approximate equipartition between particle and field energy densities.

As PKS 0637−752 is located within 15° of the southern equatorial pole, the (u, v) coverage for ground-based VLBI observations has very circular arcs. The relatively rapid motion of the HALCA satellite resulted in significantly enhanced and extended (u,v) coverage for this source. In addition, PKS 0637−752 is located within 15° of the southern ecliptic pole, meaning it is visible all year round for satellites like HALCA, which had a nominal sun-avoidance angle of 70°. Thus, regular monitoring of the source would be possible with the VSOP-2 satellite, which offers gains in sensitivity and resolution of an order of magnitude over VSOP observations (Hirabayashi et al. 2004). Such monitoring would allow tighter constraints to be placed on any non-linearities in component motions, and to better determine the range of position angles over which components are ejected. This improved understanding of the parsec-scale jet kinematics will aid in the interpretation of the multi-wavelength emission from the kpc-scale jet components, and in turn on the important question of the matter content of the jet itself.

We gratefully acknowledge the VSOP Project, which is led by the Institute of Space and Astronautical Science, Japan Aerospace Exploration Agency, in cooperation with many organizations and radio telescopes around the world. The Australia Telescope is funded by the Commonwealth of Australia for operation as a National Facility managed by CSIRO. The referee is thanked for suggestions which resulted in an improved paper.

References

Beasley, A. J., Conway, J. E., Booth, R. S., Nyman, L.-A., & Holdaway, M. 1997, A&AS, 124, 469
Bechtold, J., Dobrzycki, A., Wilden, B., Morita, M., Scott, J., Dobrzycka, D., Tran, K.-V., & Aldcroft, T. L. 2002, ApJS, 140, 143
Bennett, C. L., et al. 2003, ApJS, 148, 97
Celotti, A., Ghisellini, G., & Chiaberge, M. 2001, MNRAS, 321, L1
Chartas, G., et al. 2000, ApJ, 542, 655
Fichtel, C. E., et al. 1994, ApJS, 94, 551
Garcia, A., Sodré, L., Jr, Jablonski, F. J., & Terlevich, R. J. 1999, MNRAS, 309, 803
Georganopoulos, M., Kazanas, D., Perlman, E., & Stecker, F. W. 2005, ApJ, 625, 656
Hirabayashi, H., et al. 2000, PASJ, 52, 955
Hirabayashi, H., et al. 2004, Proc. SPIE, 5487, 1646
Homan, D. C., Lister, M. L., Kellermann, K. I., Cohen, M. H., Ros, E., Zensus, J. A., Kadler, M., & Vermeulen, R. C. 2003, ApJ, 589, L9
Jorstad, S. G., Marscher, A. P., Mattox, J. R., Aller, M. F., Aller, H. D., Wehrle, A. E., & Bloom, S. D. 2001, ApJ, 556, 738
Kataoka, J., Tanihata, C., Kawai, N., Takahara, F., Takahashi, T., Edwards, P. G., & Makino, F. 2002, MNRAS, 336, 932
Kellermann, K. I., et al. 2004, ApJ, 609, 539
Lovell, J. E. J., et al. 2000, in Astrophysical Phenomena Revealed by Space VLBI, ed. H. Hirabayashi, P. G. Edwards, & D. W. Murphy (Sagamihara: ISAS), 215
Marshall, H. L., et al. 2005, ApJS, 156, 13
Ojha, R., et al. 2004, AJ, 127, 3609
Piner, B. G., Edwards, P. G., Wehrle, A. E., Hirabayashi, H., Lovell, J. E. J., & Unwin, S. C. 2000, ApJ, 537, 91
Piner, B. G., & Kingham, K. A. 1998, ApJ, 507, 706
Sambruna, R. M., Gambill, J. K., Maraschi, L., Tavecchio, F., Cerutti, R., Cheung, C. C., Urry, C. M., & Chartas, G. 2004, ApJ, 608, 698
Schilizzi, R. T. 2004, Proc. SPIE, 5489, 62
Schwartz, D. A., et al. 2000, ApJ, 540, 69
Tavecchio, F., Maraschi, L., Sambruna, R. M., & Urry, C. M. 2000, ApJ, 544, L23
Tingay, S. J., et al., 1998, ApJ, 497, 594
Tingay, S. J., et al., 2000, Adv. Space Res., 26, 677
Tingay, S. J., et al., 2002, ApJS, 141, 311
Tingay, S. J., Jauncey, D. L., King, E. A., Tzioumis, A. K., Lovell, J. E. J., & Edwards, P. G. 2003, PASJ, 55, 351
Tornikoski, M., et al. 1996, A&AS, 116, 157
Uchiyama, Y., Urry, C. M., Van Duyne, J., Cheung, C. C., Sambruna, R. M., Takahashi, T., Tavecchio, F., & Maraschi, L. 2005, ApJ, 631, L113
Yaqoob, T., George, I. M., Turner, T. J., Nandra, K., Ptak, A., & Serlemitsos, P. J. 1998, ApJ, 505, L87

Downloaded from https://academic.oup.com/pasj/article/58/2/233/1514666 by guest on 04 November 2020